Mechanistic Investigations of a Ribozyme Derived from the Tetrahymena Group I Intron: Insights into Catalysis and the Second Step of Self-Splicing†

Rui Mei and Daniel Herschlag*

Department of Biochemistry, Beckman Center B400, Stanford University, Stanford, California 94305-5307

Received November 21, 1995; Revised Manuscript Received February 8, 1996⊗

ABSTRACT: Self-splicing of *Tetrahymena* pre-rRNA proceeds in two consecutive phosphoryl transesterification steps. One major difference between these steps is that in the first an exogenous guanosine (G) binds to the active site, while in the second the 3′-terminal G414 residue of the intron binds. The first step has been extensively characterized in studies of the L-21ScaI ribozyme, which uses exogenous G as a nucleophile. In this study, mechanistic features involved in the second step are investigated by using the L-21G414 ribozyme. The L-21G414 reaction has been studied in both directions, with G414 acting as a leaving group in the second step and a nucleophile in its reverse. The rate constant of chemical step is the same with exogenous G bound to the L-21ScaI ribozyme and with the intramolecular guanosine residue of the L-21G414 ribozyme. The result supports the previously proposed single G-binding site model and further suggests that the orientation of the bound G and the overall active site structure is the same in both steps of the splicing reaction. An evolutionary rationale for the use of exogenous G in the first step is also presented. The results suggest that the L-21G414 ribozyme exists predominantly with the 3′-terminal G414 docked into the G-binding site. This docking is destabilized by ~100-fold when G414 is attached to an electron-withdrawing pA group. The internal equilibrium with $K_{int} = 0.7$ for the ribozyme reaction indicates that bound substrate and product are thermodynamically matched and is consistent with a degree of symmetry within the active site. These observations are consistent with the presence of a second Mg ion in the active site. Finally, the slow dissociation of a 5′ exon analog relative to a ligated exon analog from the L-21G414 ribozyme suggests a kinetic mechanism for ensuring efficient ligation of exons and raises new questions about the overall self-splicing reaction.

Self-splicing of the *Tetrahymena* pre-rRNA proceeds in two consecutive phosphoryl transesterification steps (Figure 1A; Cech, 1990). In the first step, an exogenous guanosine (G)[1] acting as a nucleophile attacks the 5′ splice site, leaving the 5′ exon with a 3′-hydroxyl terminus. In the second step, the 3′-terminal residue of the intron, G414, binds to the active site, and its 3′ phosphoryl group is attacked by the 3′-hydroxyl of the 5′ exon. This gives ligated exons and the free intron.

The first step of self-splicing has been studied by using a shortened version of the intron. This version, referred to as the L-21ScaI ribozyme (Figure 2B), has the first 21 and last 5 nucleotides removed and mimics the first step of the self-splicing reaction (Figure 1B). Extensive studies of the L-21ScaI ribozyme have provided insights into the mechanism of RNA catalysis and the first step of self-splicing (Cech et al., 1992).

The second step of self-splicing, however, has not been characterized in as much detail. Several components have been shown to be involved in this step (Figure 2A). Guanosine is universally conserved as the 3′-terminal residue of group I intron, specifying the 3′ splice site (G414 for *Tetrahymena* pre-rRNA) (Waring & Davies, 1984; Michel et al., 1982; Michel & Westhof, 1990). The helix P9.0 is comprised of two base pairs between the nucleotides immediately preceding the 3′-terminal G and two nucleotides in the core of the intron. It presumably assists in positioning the 3′-terminal G in its binding site (Burke et al., 1990; Michel et al., 1989). The helix P10 is comprised of base pairs between the 3′ exon and internal guide sequence (IGS). As the IGS also binds the 5′ exon, P10 presumably aligns the exons for ligation (Burke et al., 1990; Waring & Davies, 1984; Michel & Westhof, 1990).

As an initial approach toward a detailed understanding of the second step, a simplified model system was employed. We used a ribozyme containing both the 3′-terminal G414 and the helix P9.0, referred to as L-21G414 or E^{G414} (Figure 2C). This ribozyme uses the 3′-terminal G414 as an intramolecular nucleophile to catalyze the site-specific cleav-

† This work was supported by NIH Grant GM49243 to D.H. D.H. is a Lucille P. Markey Scholar in Biomedical Sciences and a Searle Scholar (Chicago Community Trust). R.M. was supported by an NIH postdoctoral fellowship.

* To whom correspondence should be addressed. Phone: 415-723-9442. Fax: 415-723-6783. E-mail: herschla@cmgm.stanford.edu.

⊗ Abstract published in *Advance ACS Abstracts,* April 15, 1996.

[1] Abbreviations: P, oligonucleotides of the sequence CCCUCU, without specification of the sugar identity; P*, 5′-^{32}P-labeled product, −1d,rP* or rP*; S, oligonucleotides of the sequence CCCUCUAAAAA, without specification of the sugar identity; S*, 5′-^{32}P-labeled substrate, −1d,rS* or rS*; rS, rP, all-ribose substrate (rCrCrCrUrCrUrArArArArA) and product (rCrCrCrUrCrU), respectively; −1d,rS, −1d,rP chimeric substrate and product with a single deoxyribose residue at position −1 from the cleavage site and all others ribose residues, rCrCrCrUrCdU-rArArArArA and rCrCrCrUrCdU, respectively; E^{G414}, the L-21G414 ribozyme with a 3′-guanosine residue; E^{G414A_5}, the L-21G414 ribozyme with an AAAAA tail attached to G414; E^{ScaI}, the L-21ScaI ribozyme; G, guanosine; G414, 3′-terminal guanosine residue of the *Tetrahymena* intron; IGS, internal guide sequence; IVS, intervening sequence; CHES, (cyclohexylamino)ethanesulfonic acid; EDTA, (ethylenedinitrilo)tetraacetic acid; EPPS, *N*-2-(hydroxyethyl)piperazine-*N*-3-propanesulfonic acid; HEPES, *N*-(2-hydroxylethyl)piperazine-*N*′-(2-ethanesulfonic acid); MES, 2-(*N*-morpholino)ethanesulfonic acid; Tris, Tris(hydroxymethyl)-aminomethane.

S0006-2960(95)02765-6 CCC: $12.00

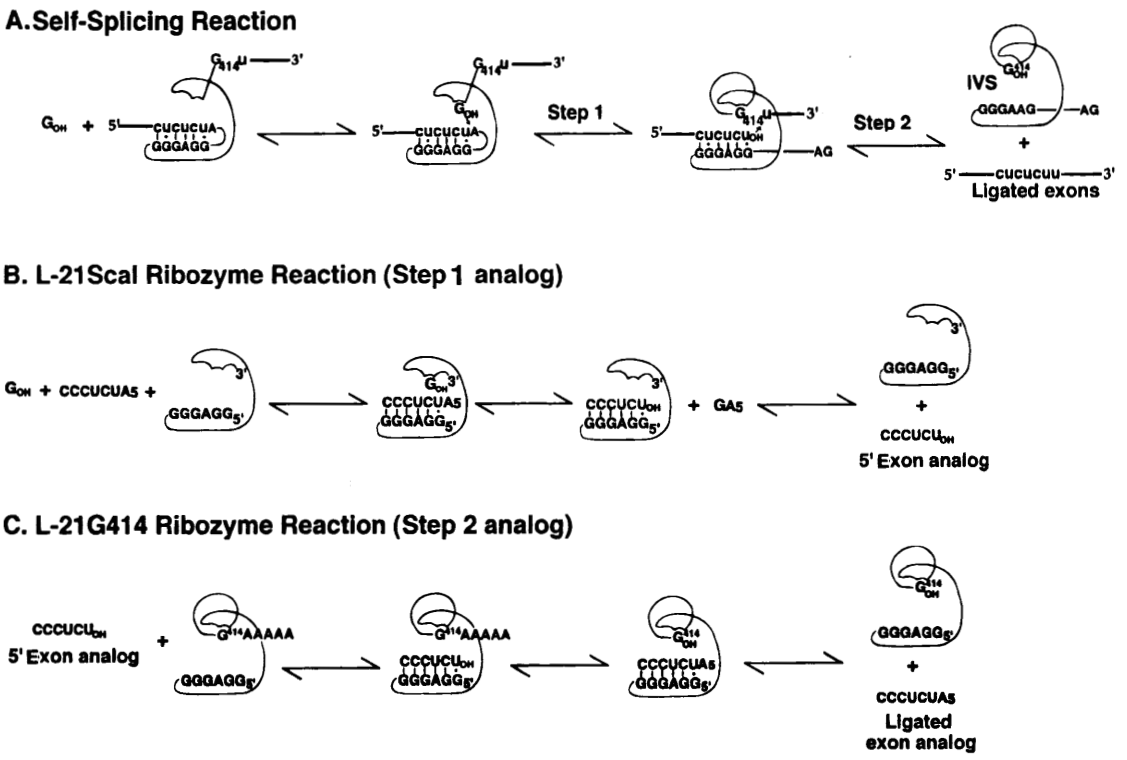

FIGURE 1: *Tetrahymena* pre-rRNA self-splicing (A) and ribozyme reactions (B and C). The lowercase letters and thick lines represent exon sequences, and the uppercase letters and thin lines represent intron sequences. The self-splicing of pre-rRNA undergoes two transesterification steps. The L-21ScaI (E^{ScaI}) and L-21G414 (E^{G414}) ribozymes mimic the first and second steps of the splicing reaction, respectively. The differences between the intron and ribozymes are depicted in Figure 2. For simplicity, a conformational change required to link the two chemical steps in self-splicing (A), in which the exogenously added G leaves the active site and G414 at the 3′ splice site enters the active site, is not shown as a distinct step.

age of oligonucleotide substrates provided in *trans* (Figure 1C; Zaug & Cech, 1986a,b). A kinetic and thermodynamic framework for the L-21G414 ribozyme reaction in both directions has been established in this study. This framework provides mechanistic insights for understanding RNA catalysis and the self-splicing reaction. A kinetic model for ensuring efficient exon ligation is proposed from this framework. This model raises new questions concerning how rapid and efficient self-splicing is accomplished. As the L-21G414 ribozyme has been used for *in vitro* evolution of new RNA catalysts (Robertson & Joyce, 1990; Lehman & Joyce, 1993; Tsang & Joyce, 1994), the framework presented herein will also provide a starting point for analysis of functional consequences of molecular changes in these evolved ribozymes.

MATERIALS AND METHODS

L-21G414 Ribozyme. The L-21G414 ribozyme was prepared by *in vitro* transcription of *Hin*dIII-digested plasmid pT7L-21 with T7 RNA polymerase as described previously (Zaug et al., 1988). The transcripts were then incubated for 60 min at pH 9.0 to generate the 3′-terminal G414 with a free 3′-hydroxyl group via site-specific hydrolysis and were purified by gel electrophoresis (4% polyacrylamide/8 M urea) and gel filtration (Zaug & Cech, 1986a,b).

Oligonucleotide and Ribozyme End Labeling. Oligonucleotides were made by solid-phase synthesis (provided by Ribozyme Pharmaceuticals, Inc. or used and characterized in previous studies). For 5′-labeling, oligonucleotides were labeled with [γ-^{32}P]ATP by T4 polynucleotide kinase (Zaug et al., 1988). For 3′-labeling, oligonucleotides were labeled with [5′-^{32}P]adenosine 3′,5′-bisphosphate (pAp) by T4 RNA ligase (Bruce & Uhlenbeck, 1978). The labeled oligonucleotides were purified by nondenaturing polyacrylamide gel electrophoresis (Herschlag et al., 1993a). Ribozyme labeled with ^{32}P on its 3′ end was produced by incubating the ribozyme with the 3′-labeled oligonucleotide for 30 min at 50 °C in the presence of 10 mM $MgCl_2$ and 50 mM sodium MES (pH 6.8). The labeled ribozyme was then purified by gel electrophoresis (4% polyacrylamide/8 M urea).

General Kinetic Measurements. All reactions were performed under single-turnover conditions with E^{G414} in excess of S*, essentially as described previously (Herschlag & Cech, 1990; Herschlag et al., 1993a). The ribozyme was preincubated with 10 mM $MgCl_2$ and 50 mM sodium MES, pH 6.8, at 50 °C for 30 min. The preincubation promotes folding of the ribozyme into an active conformation, as previously observed for the L-21ScaI ribozyme. Cleavage reactions were initiated by addition of S* (~0.1 nM) and were quenched at particular times by addition of a stop solution containing 20 mM EDTA in 90% formamide with 0.005% xylene cyanol, 0.01% bromophenol blue, and 1 mM Tris (pH 7.5). S* and P* were separated by electrophoresis on a 20 %/7 M urea polyacrylamide gel, and their identities were confirmed by migration relative to known standards. The slow migration of the product from reaction with 3′-labeled S is consistent with formation of the 3′ product, $E^{G414A_5p^*A_p}$. The ratio of S* and P* at each time point was quantitated using a Molecular Dynamics PhosphorImager. Data were analyzed by nonlinear least-squares fitting (KaleidaGraph by Synergy Software, Reading, PA). Reactions followed good first-order kinetics, unless stated otherwise. Errors are within 2-fold, based on repeated experiments as well as on measurements using independent experimental

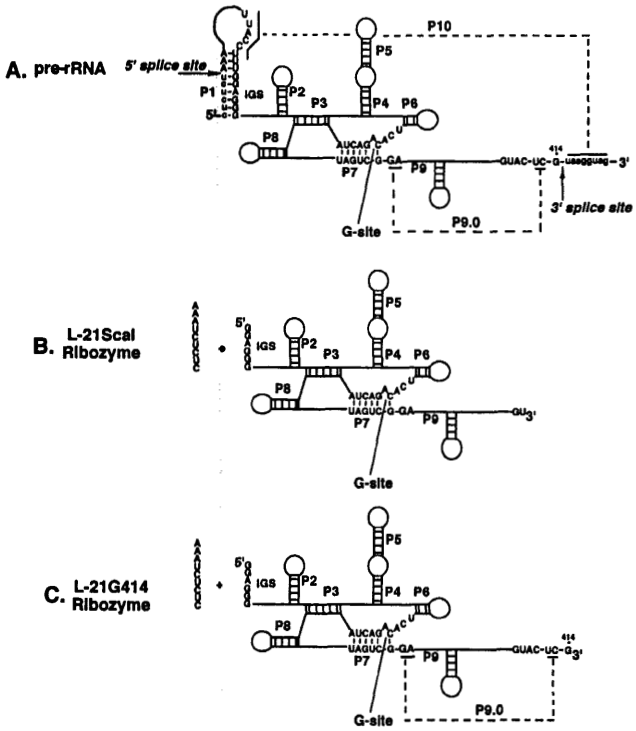

FIGURE 2: Secondary structure of *Tetrahymena* pre-rRNA group I intron (A) and ribozymes derived from it (B and C). The exon sequences are depicted by the lowercase letters, and the intron sequences by the uppercase letters and thin lines. To produce the L-21ScaI ribozyme (B), the first 21 nucleotides from the 5′ side and the five nucleotides from the 3′ end were removed from the intron; the ribozyme uses exogenous G as an intermolecular nucleophile. To produce the L-21G414 ribozyme (C), only the first 21 nucleotides were removed; the ribozyme uses its 3′-terminal G414 as an intramolecular nucleophile.

approaches. For experiments requiring saturating concentrations of E^{G414}, saturation was verified by showing that the observed rate constants and reaction extents remained constant as $[E^{G414}]$ was varied from 100 to 500 nM.

Pulse–Chase Experiment. Pulse–chase experiments (Rose et al., 1974; Herschlag & Cech, 1990) were extensively used in this study. The advantage of this technique is that the change in reaction conditions in the chase step allows isolation of individual reaction steps. In a typical experiment, the reaction was initiated by addition of S* following preincubation of E^{G414}, and the initial phase of the reaction was allowed to proceed for a specified time (t_1). The reaction mixture (typically containing 100 nM E^{G414} and 0.1 nM S*) was then diluted 10-fold with a chase solution containing 5 μM unlabeled rP in the appropriate buffer. The 10-fold dilution of E^{G414} and the addition of a large excess of unlabeled rP were designed to prevent free S* or P* from rebinding to E^{G414} ($[rP]/[E^{G414}] = 500$). The effectiveness of the chase solution was tested by control experiments in which S* was added with the chase solution; no cleavage was observed, indicating that the chase was effective. In addition, when S* and the large excess of unlabeled rP were added along with the chase solution, no binding of S* to E^{G414} was observed in a gel mobility shift assay (see below).

Gel Mobility Shift Assay To Follow Dissociation of S and P. E^{G414}, after preincubation, was mixed with −1d,rS* to allow binding and equilibration of the bound species at 50 °C (t_1 = 10 min). A 10-fold excess of the chase solution containing unlabeled rP in reaction buffer at 50 °C was then added, and aliquots were removed at specified times. The aliquots were immediately added to a loading buffer containing 40% glycerol and 0.5% xylene cyanol and carefully loaded onto a 10% native polyacrylamide gel while the gel was running (Pyle et al., 1990). The gel running buffer contained 100 mM Tris-HEPES (34 mM Tris and 66 mM HEPES, pH 7.5), 0.1 mM EDTA, and 10 mM $MgCl_2$, and the running temperature was maintained at 10 °C to limit further dissociation. Control experiments demonstrated that the complexes remain intact during loading and electrophoresis. Ribozyme with bound −1d,rS* or −1d,rP* appeared as a single high molecular weight band, whereas free −1d,rS* and −1d,rP* appeared as distinct low molecular weight bands. The identity of these species was confirmed by comigration with −1d,rS* and −1d,rP* standards. Analogous gel mobility shift assays were performed to determine the rate constant for dissociation of −1d,rP* from the E^{G414}/−1d,rP* complex.

Scheme 1[a]

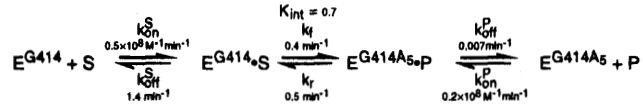

[a] S = −1d,rS; P = −1d,rP; 50 °C, pH 6.8, 10 mM $MgCl_2$.

Test of Active Population of the L-21G414 Ribozyme. The folding of E^{G414} was extensively tested by changing the concentration of $MgCl_2$ and the temperature during the preincubation period. An optimum folding condition was chosen in which the ribozyme was preincubated with 10 mM $MgCl_2$ at 50 °C for 30 min. Longer incubations gave no increase in rate. The leveling off of the reaction extent at ~40% (see Results) was not a result of inactive ribozyme, as reactions were carried out with a large excess of E^{G414} over S*, and increasing the E^{G414} concentration or decreasing the −1d,rS* concentration did not increase the extent of reaction. The amount of active ribozyme was tested by titrating the ribozyme with unlabeled S and following the reaction with a trace amount of S*. Side-by-side comparison of E^{G414} and E^{ScaI} preparations indicated that both are fully active (>80%). Finally, no degraded E^{G414} was observed upon electrophoresis of 5′-end-labeled E^{G414} in 4% polyacrylamide/8 M urea gels.

RESULTS

In contrast to the L-21ScaI ribozyme, the L-21G414 ribozyme uses the 3′-terminal G414 residue as an intramolecular nucleophile to initiate the transesterification reaction (Figure 1B,C). For the L-21ScaI ribozyme, the rate of the chemical reaction can be controlled by varying the concentration of exogenous nucleophile. However, in the case of L-21G414, the nucleophile is covalently linked to the ribozyme. Thus, an alternative approach using an intrinsically slower substrate was taken in this study. A deoxyribose substitution at the cleavage site, −1d,rS, reduces the rate of the chemical step of the L-21ScaI ribozyme reaction about 10^3-fold, without having a significant effect on binding (Herschlag et al., 1993b). Several specific experiments suggest that the all-ribose substrate also behaves similarly in both ribozyme reactions (*vide infra* and unpublished results).

Scheme 1 summarizes the results of the kinetic and thermodynamic study described in following sections for the L-21G414 ribozyme, and Table 1 compares these results with

Table 1: Comparison of Rate Constants for the L-21G414 and L-21ScaI Ribozymes

rate constant[a]	L-21G414[b]	L-21ScaI[c]
k_{on}^{S} (M^{-1} min^{-1})	0.5×10^8	1×10^8
k_{off}^{S} (min^{-1})	1.4	0.2
k_f (min^{-1})	0.4	0.4
k_r (min^{-1})	0.5	ND
k_{off}^{P} (min^{-1})	0.007	ND
$k_{off}^{P'}$ (min^{-1})[d]	0.1	0.3
k_{on}^{P} (M^{-1} min^{-1})	0.2×10^8	0.6×10^8

[a] Reaction of −1d,rS at 50 °C with 50 mM sodium MES and 10 mM $MgCl_2$, pH 6.8. [b] Rate constants for the L-21G414 ribozyme are defined in Scheme 1 and were obtained as described in the text. [c] Rate constants for the L-21ScaI ribozyme are defined as in the following equation:

$$E{\cdot}G + S \underset{k_{off}^{S}}{\overset{k_{on}^{S}}{\rightleftharpoons}} E{\cdot}S{\cdot}G \xrightarrow{k_f} E{\cdot}P{\cdot}GA_5 \underset{k_{on}^{P}}{\overset{k_{off}^{P}}{\rightleftharpoons}} E + P$$

The rate constants were obtained as follows: k_{on}^{S}, from Herschlag et al. (1993b); k_{off}^{S}, from the value of 1 min^{-1} for dissociation of −1d,rS from E^{ScaI} (Herschlag et al., 1993b); this value was corrected by 5-fold to account for the slower dissociation of S in the presence of bound G (McConnell et al., 1993). k_f was measured side-by-side with E^{G414} in this study; the value agrees well with the literature values of $k_f = 0.55$ min^{-1} (pH 7.0; McConnell et al., 1993) and 0.29 min^{-1} (pH 6.6; Knitt et al., 1994). k_r and k_{off}^{P} could not be determined, as the weak binding of GA_5 to the ribozyme prevents saturation from being achieved (T. S. McConnell, D. Herschlag, and T. R. Cech, unpublished results). k'^{P}_{off} for −1d,rP was estimated from the rate constant of 0.12 min^{-1} for dissociation of rP from E^{ScaI} in the absence of bound G (G. J. Narlikar and D. Herschlag, unpublished results), and a 2.5-fold increase in the rate constant for dissociation from the weaker duplex stability with a deoxyribose residue at U(−1) (Bevilacqua & Turner, 1991; G. J. Narlikar and D. Herschlag, manuscript in preparation). Though G and the oligonucleotide product bind anticooperatively, the effect is small (~2-fold) and may in part be reflected in k_{on} rather than k_{off} (Bevilacqua et al., 1993; McConnell et al., 1993). Therefore, no correction was made in k'^{P}_{off} for this effect. This estimate for k'^{P}_{off} is expected to be accurate to within 3-fold. k_{on}^{P} was measured for rP in the absence of bound GA_5 (G. J. Narlikar and D. Herschlag, unpublished results); single deoxyribose substitutions do not significantly affect rate constants for binding to the ribozyme (Herschlag et al., 1993a,b). In addition, though bound GA_5 was not present, bound G has less than a 2-fold effect on the rate of S binding (Herschlag & Cech, 1990; McConnell et al., 1993; D. S. Knitt, G. J. Narlikar, and D. Herschlag, unpublished results). [d] The rate constant for dissociation of −1d,rP from either E^{G414} or $E^{ScaI}_{.G}$, i.e., with intramolecular or exogenous G occupying the guanosine binding site.

those obtained previously for the L-21ScaI ribozyme. For simplicity, E^{G414} and E^{ScaI} refer to the L-21G414 and L-21ScaI ribozymes, respectively, S the substrate, either −1d,rS or the all-ribose substrate rS, and P the product, either −1d,rP or rP.

Observation of an Internal Equilibrium for the L-21G414 Ribozyme Reaction

The chemical step of the E^{G414} reaction was isolated under single-turnover conditions in the presence of excess, saturating E^{G414}, which allows rapid and complete formation of the $E^{G414}{\cdot}S^*$ complex (eq 1a).

$$E^{G414}{\cdot}p^*r(CCCUC)dUr(AAAAA) \overset{k_{obs}}{\rightleftharpoons} E^{G414A_5}{\cdot}p^*r(CCCUC)dU \quad (1a)$$

$$E^{G414}{\cdot}r(CCCUC)dUr(AAAAA)p^*Ap \overset{k_{obs}}{\rightleftharpoons} E^{G414A_5p^*Ap}{\cdot}r(CCCUC)dU \quad (1b)$$

The reaction proceeded to a plateau with 0.6 of the 5′-labeled S* remaining, with an observed rate constant k_{obs} = 0.90 min^{-1} (Figure 3, open symbols). The remaining 0.4 of the radioactivity was present as the 5′ product P* (eq 1a), but the 3′ product, predicted to be E^{G414A_5}, is not labeled. To identify the 3′ product and test this result further, S* labeled at its 3′ end was used (eq 1b). This reaction also gave a plateau with 0.6 S* remaining, while 0.4 of it was converted to the 3′ product, $E^{G414A_5p^*Ap}$ (Figure 3, closed symbols). Moreover, the observed rate constant of 0.95 min^{-1} was the same, within experimental error, as that obtained with 5′-labeled S*. A similar plateau, with 0.4 S* remaining and 0.6 converted to P*, was also observed for the reaction of rS. However, the reaction was too fast to determine the observed rate constant (not shown), as predicted from results with E^{ScaI} (Herschlag et al., 1993b).

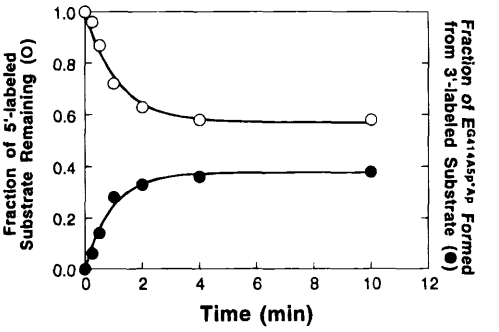

FIGURE 3: L-21G414 ribozyme reaction reaches a plateau. Reactions of 100 nM E^{G414} with 0.1 nM 5′-labeled −1d,rS (p*CCCUCdUA$_5$) (○) or 3′-labeled −1d,rS (CCCUCdUA$_5$p*Ap) (●) with 10 mM $MgCl_2$ and 50 mM sodium MES (pH 6.8) at 50 °C. Lines represent nonlinear least-squares fits to the data with k_{obs} = 0.90 min^{-1} and an endpoint of 0.6 for disappearance of the 5′-labeled substrate (○) and k_{obs} = 0.95 min^{-1} and an endpoint of 0.4 for formation of the 3′-labeled product, $E^{G414A_5p^*Ap}$, from the 3′-labeled substrate (●).

Evidence for the Establishment of an Internal Equilibrium (K_{int}). The plateau remained constant over the time course of Figure 3, suggesting that an equilibrium was reached. The final extent of reaction did not increase with increasing ribozyme concentration, suggesting that the plateau represents the internal equilibrium of bound S and P (data not shown). The pulse−chase experiment described below directly tested the existence of the internal equilibrium (K_{int}, Scheme 1). The results show that P* dissociation is slow (compared to S* dissociation) and that bound P* can be converted back to S* in the reverse reaction, providing evidence that the internal equilibrium was indeed established.

In the pulse−chase experiment, time was first allowed for equilibration between bound −1d,rS* and −1d,rP* (Figure 4A, t_1). The reaction reached the plateau shown in Figure 3, with the fraction of S* remaining nearly constant between 10 and 60 min (Figure 4B, closed symbols). During this plateau period (at t_1 = 30 min), a chase solution containing a large excess of unlabeled P was added to prevent rebinding of S* and P* that has dissociated from the ribozyme before or during t_2 (eq 2). Addition of the chase resulted in the

$$\begin{array}{ccccccc} E^{G414A_5} + P^* & \underset{\text{slow}}{\overset{k_{off}^{P}}{\leftarrow}} & E^{G414A_5}{\cdot}P^* & \rightleftharpoons & E^{G414}{\cdot}S^* & \xrightarrow{k_{off}^{S}} & E^{G414} + S^* \\ \downarrow P,\text{trap} & & & & & & \downarrow P,\text{trap} \\ E^{G414A_5}{\cdot}P + P^* & & & & & & E^{G414}{\cdot}P + S^* \end{array} \quad (2)$$

near quantitative regeneration of S* during t_2 (Figure 4B, open symbols). This result demonstrates that nearly all of the P* remained bound during t_1 and that the bound P* was

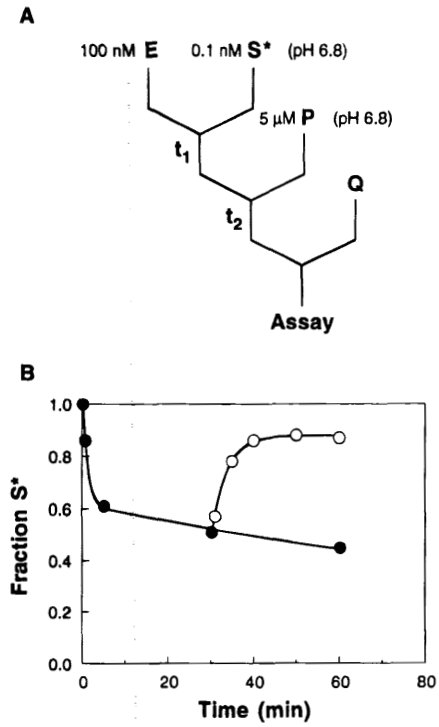

FIGURE 4: Regeneration of S* provides evidence for the establishment of the internal equilibrium (K_{int}). (A) Outline of the pulse chase protocol. E^{G414} (100 nM) was mixed with ~0.1 nM 5′-labeled −1d,rS* for t_1 = 30 min (10 mM $MgCl_2$ and 50 mM sodium MES, pH 6.8, at 50 °C). The reaction mixture was then diluted 10-fold by a chase solution containing 5 μM unlabeled rP to initiate the t_2 phase of the reaction. (B) The disappearance of S* during t_1 (●), and its regeneration during t_2 (○). The lines represent nonlinear least-squares fits to the data. The regeneration of S* during t_2 (○) follows a single first-order rate constant with k_{obs} = 0.28 min^{-1} and an endpoint of 0.88 S*. The disappearance of S* during t_1 (●, additional time points not shown) is fit to two successive exponential functions according to the equation $S_t = S_1e^{-k_1t} + S_2e^{-k_2t}$, with k_1 = 0.88 min^{-1}, k_2 = 0.005 min^{-1}, S_1 = 0.38, and S_2 = 0.62. The initial fast phase represents establishment of the internal equilibrium and the second phase the slow dissociation of P (see text). (These values are in reasonable agreement with those obtained via independent approaches.)

competent to participate in the reverse reaction. Independent evidence for this equilibration was also obtained by experiments in which the equilibrium was perturbed in both directions by changing the identity of the divalent metal ion present (R. Mei and D. Herschlag, unpublished results).

Rate and Equilibrium Constants for the Internal Equilibrium. The data of Figure 3 and analogous experiments give values of $K_{int} = [E^{G414A_5}\cdot P]/[E^{G414}\cdot S] = 0.70 \pm 0.03$ and $k_{obs} = 0.99 \pm 0.24$ min^{-1}. The reaction is an approach to the internal equilibrium so that $k_{obs} = k_f + k_r$ (Scheme 1). The rate constants k_f = 0.41 min^{-1} and k_r = 0.58 min^{-1} were calculated from k_{obs} and K_{int} (= k_f/k_r) using the values obtained above. The agreement of the calculated rate constants with values determined directly provides further evidence for this equilibrium (see below).

Equilibrium Experiments Suggest That P Dissociates Much More Slowly Than S. In the pulse−chase experiment of Figure 4, if S* and P* dissociated from the ribozyme at the same rate, the addition of chase would have resulted in irreversible dissociation of both S* and P* so that the ratio of S* and P* would have remained unchanged (eq 2). On the other hand, if P* dissociates much more slowly than S*, only S* would dissociate and P* that remains bound would be converted to S* via the reverse reaction and subsequently dissociate, giving regeneration of S* as observed in Figure 4B (open symbols). Thus, this increase in S* following the chase suggests that P* dissociation from the ribozyme is much slower than that of S*.

The results shown in Figure 4 were unexpected based on previous results with the L-21ScaI ribozyme (E^{ScaI}). The halftime for dissociation of −1d,rP from E^{ScaI} is ~5 min (Herschlag & Cech, 1990; Herschlag et al., 1993b; G. J. Narlikar, D. S. Knitt, and D. Herschlag, unpublished results). We therefore expected that after 30 min most of the P* would have dissociated from E^{G414A_5} and been trapped in a nonreactive complex by the large excess of free E^{G414} present during t_1 (eq 3).[2] In contrast, if S* dissociates it can rapidly

$$E^{G414} + S^* \overset{k_{off}^S}{\rightleftharpoons} [E^{G414}\cdot S^* \rightleftharpoons E^{G414A_5}\cdot P^*] \overset{k_{off}^P}{\dashrightarrow} E^{G414A_5} + P^* \quad (3)$$

E^{G414} → $E^{G414}\cdot P^*$ (P* is trapped)

rebind to the large excess of E^{G414} and react again. Thus, the reaction was expected to proceed to completion.

The observation that the plateau remains nearly constant until 60 min (Figure 4B, closed symbols) suggests that P dissociates slowly, as does the observation that S* can be nearly quantitatively regenerated during the chase (Figure 4B, open symbols). Moreover, the dissociation rate constants of −1d,rP and −1d,rS from E^{ScaI} are similar, with the product dissociating only ~3-fold more slowly (Herschlag et al., 1993a). The observed rate of 0.29 min^{-1} for S* regeneration (Figure 4B) provides an estimate for the rate constant for −1d,rS dissociation from E^{G414} of $k_{off}^S \approx 1.2$ min^{-1} [k_{off}^S is calculated from $k_{obs} = (k_r k_{off}^S)/(k_f + k_r + k_{off}^S)$, which was derived from eq 2, using k_{obs} = 0.29 min^{-1}, k_f = 0.41 min^{-1}, and k_r = 0.58 min^{-1}]. This rate constant is, in fact, larger than the value obtained with E^{ScaI} (Table 1), suggesting that the G414-containing ribozyme slows dissociation of P but not S.

In summary, the above results indicate that an equilibrium is established between $E^{G414}\cdot S$ and $E^{G414A_5}\cdot P$. Estimates were obtained for the equilibrium constant (K_{int}), the rate constants for the forward and reverse of the chemical step (k_f and k_r), and the rate constant for dissociation of S (k_{off}^S). In addition, the dissociation of P from $E^{G414A_5}\cdot P$ was predicted to be much slower than the dissociation of S from $E^{G414}\cdot S$. The estimates were used to design experimental tests of these initial conclusions. The following sections describe approaches to isolate individual reaction steps and directly measure their rate and equilibrium constants to confirm and extend the above conclusions.

Probing the Chemical Step. Previous work with E^{ScaI} showed that the chemical step is pH-dependent, increasing in a log-linear fashion from pH ~5−9 for −1d,rS (Herschlag & Khosla, 1994; Knitt & Herschlag, 1996). For the G414-containing ribozyme, the rate constant for approach to the internal equilibrium ($k_{obs} = k_f + k_r$; Scheme 1) was also log-

[2] This is expected because the reaction was carried out with the E^{G414} in vast excess over S* (100 nM vs 0.1 nM). This means that at most 0.1 nM E^{G414A_5} could be generated. Thus, if P* dissociated from E^{G414A_5}, it would have much greater probability of binding E^{G414} (99.9 nM) than E^{G414A_5} (<0.1 nM).

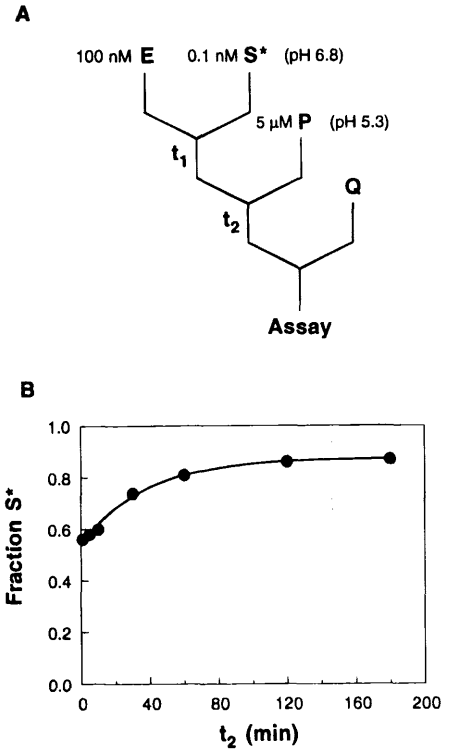

FIGURE 5: Determination of the rate constant for the reverse reaction (k_r). (A) E^{G414} was incubated with −1d,rS* for t_1 = 10 min (10 mM $MgCl_2$ and 50 mM sodium MES, pH 6.8, at 50 °C). The reaction mixture was then diluted 10-fold with a low-pH chase solution containing 5 μM unlabeled P, 10 mM $MgCl_2$, and 50 mM sodium MES (pH 5.3). (B) Time course for regeneration of S* following the chase. The curve is a nonlinear least-squares fit to the data and gives k_{obs} = 0.021 min^{-1}.

Table 2: Summary of K_{int}, k_f, and k_r Values for −1d,rS[a]

pH	k_f (min^{-1})	k_r (min^{-1})	K_{int}
5.3	0.022[b]	0.021	1.1
6.1	0.13[c]	0.16	0.79
	0.10[d]	0.19[d]	
6.8	0.41[e]	0.58[e]	0.71
	(0.57)[f]	(0.66)[f]	

[a] At 50 °C with 10 mM $MgCl_2$ and 50 mM sodium MES. [b] At pH 5.3, the chemical step is slow, so that k_{off}^P perturbs measurement of K_{int} and contributes to k_{obs}. Thus, k_f is calculated from $k_{obs} = k_f + k_r$ = 0.040 min^{-1} and k_r = 0.021 min^{-1}, with correction for the small contribution to k_{obs} from the dissociation of P (k_{off}^P = 0.007 min^{-1}). [c] Calculated from $k_{obs} = k_f + k_r$ = 0.29 min^{-1}, k_r = 0.16. [d] Calculated from $K_{int} = k_f/k_r$ = 0.79 and $k_{obs} = k_f + k_r$ = 0.29 min^{-1}. [e] Calculated from $K_{int} = k_f/k_r$ = 0.70 and $k_{obs} = k_f + k_r$ = 0.99 min^{-1}. [f] Extrapolated from the values obtained at pH 5.3 and 6.1.

linear with pH (not shown), whereas the internal equilibrium is unaffected ($K_{int} = k_f/k_r$; see below). This suggests that the chemical step is rate-limiting for reaction of −1d,rS with the G414-containing ribozyme.

The ability to manipulate the rate of the chemical step by changing pH, without perturbing binding (*vide infra*), was instrumental in isolating the reverse reaction (k_r) as well as other individual reaction steps via pulse−chase experiments employed throughout this study.

Direct Measurement of the Rate Constant for the Reverse Reaction (k_r)

A pH-drop pulse−chase experiment was designed to measure the rate constant for the reverse reaction (Figure 5A). The underlying idea was to slow k_r by lowering the pH so that it, rather than the dissociation of S, would become rate-limiting for the overall reverse reaction. An excess of E^{G414} was incubated with −1d,rS* at pH 6.8 for t_1 = 10 min to establish the internal equilibrium (eq 4; Figure 5A).

Table 3: pH Dependence of the Chemical Step (k_f) for E^{ScaI} and E^{G414} [a]

pH	k_f (min^{-1})[b] E^{ScaI}	k_f (min^{-1})[b] E^{G414}
5.3	0.011	0.014[c]
6.1	0.051	0.082
6.8	0.48	0.45

[a] E^{ScaI} and E^{G414} reactions were performed side-by-side with 10 mM $MgCl_2$ and 50 mM sodium MES at 50 °C. In the E^{ScaI} reaction, a saturating concentration (2.5 mM) of guanosine was used. [b] For E^{ScaI}, $k_{obs} = k_f$ since its reaction proceeds to completion. For E^{G414}, however, $k_{obs} = k_f + k_r$ since its reaction reaches an internal equilibrium, and k_f was calculated from $K_{int} = k_f/k_r$ and $k_{obs} = k_f + k_r$. [c] Calculated from $k_{obs} = k_f + k_r$ = 0.027 min^{-1} and $K_{int} = k_f/k_r$ = 1.1 with correction for the small contribution to k_{obs} from the dissociation of P, as in Table 2.

$$\text{during } t_1\text{: } E^{G414}\cdot S^* \overset{K_{int}}{\rightleftharpoons} E^{G414A_5}\cdot P^* \qquad (4)$$

Then, a pH 5.3 chase solution was added to the incubation mixture (t_2 = 0). This decreases the rate of the chemical conversion ~30-fold without changing the dissociation rates (*vide infra*), so that the rate-limiting step for conversion of bound P* to free S* is k_r (eq 5; $k_r \ll k_{off}^S$). Thus, the value

$$\text{during } t_2\text{: } E^{G414A_5}\cdot P^* \overset{k_r,\ \text{slow}}{\rightleftharpoons} E^{G414}\cdot S^* \overset{k_{off}^S,\ \text{fast}}{\longrightarrow} E^{G414} + S^* \qquad (5)$$

of k_{obs} = 0.021 min^{-1} for formation of S* during t_2 reflects k_r (Figure 5B; Table 2, pH 5.3). A value of k_r = 0.16 min^{-1} was obtained from an analogous experiment at pH 6.1 (Table 2). However, k_r at pH 6.8 could not be directly measured because $k_r \approx k_{off}^S$ at this pH so that k_{obs} reflects a combination of rate constants. The value of k_r = 0.58 min^{-1} at pH 6.8 was calculated from the equilibrium constant for the internal equilibrium and the observed rate constant for the approach to this equilibrium (Table 2). This value is in reasonable agreement with the value of k_r = 0.66 min^{-1} at pH 6.8 obtained from extrapolation of the values at pH 5.3 and 6.1 to pH 6.8, using the log-linear pH dependence.

The value of the internal equilibrium and the rate constant for approach to the equilibrium were also determined at each pH to validate and extend the above conclusions (Table 2). These results indicate that both k_r and k_f increase log-linearly with pH and that K_{int} is pH-independent.

Comparison of the Rate of the Chemical Step for E^{G414} and E^{ScaI}. The rate of the chemical step for the L-21G414 and L-21ScaI ribozymes were compared side-by-side (eq 6a,b). The rate constants (k_f) are the same, within error, for

$$E^{G414}\cdot S \xrightarrow{k_f} E^{G414A_5}\cdot P \qquad (6a)$$

$$E^{ScaI}\cdot G\cdot S \xrightarrow{k_f} E^{ScaI}\cdot GA_5\cdot P \qquad (6b)$$

−1d,rS at various pH values (Table 3). For rS, accurate rate

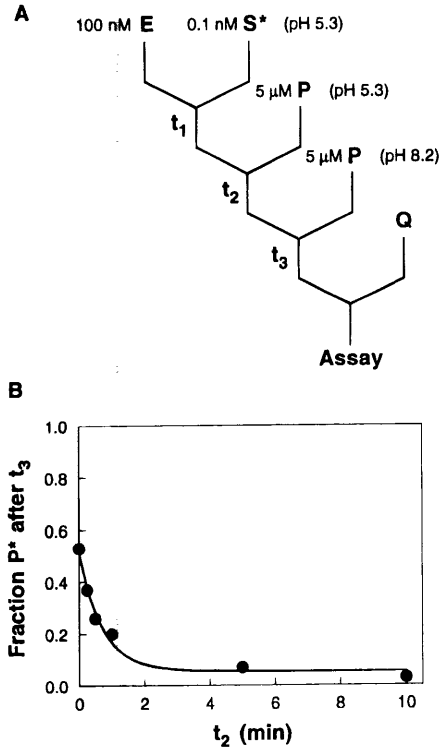

FIGURE 6: Determination of the rate constant for the dissociation of substrate (k_{off}^{S}). (A) E^{G414} was incubated with −1d,rS* for t_1 = 1 min (10 mM $MgCl_2$ and 50 mM sodium MES, pH 5.3), followed by a 2-fold dilution with a chase solution containing 50 μM unlabeled P, 10 mM $MgCl_2$, and 50 mM MES, pH 5.3, at various times t_2. The reaction mixtures were then diluted 10-fold with a second chase solution at pH 8.2 (5 μM unlabeled P, 10 mM $MgCl_2$, and 50 mM sodium EPPS) for t_3 = 30 s, enough time for conversion of S* to P* but not for dissociation of P*. (B) The fraction of P* formed during t_3 as a function of the t_2 incubation time (●). Control experiments showed that there is <0.1 formation of P* during t_2. The line represents a nonlinear least-squares fit to the data giving a rate constant of k_{off}^{S} = 1.4 min^{-1}. The amount of P* formed during t_3 is less than 1.0 even when S* has had no time to dissociate (t_2 = 0). This is because the reverse of the chemical step (k_r) also occurs during t_3 to rapidly establish the internal equilibrium. The P* formed during t_3 is proportional to the amount of S* that remains bound at the end of each t_2: $[S^*]_{t_2} = [P^*]_{t_3}(1 + K_{int})/K_{int}$, so that the decrease in P* formed with increasing t_2 gives the rate constant for dissociation of S, k_{off}^{S}.

constants can only be measured by manual pipetting at low pH and low temperature. Similar values of k_f = 0.10 and0.11 min^{-1} were obtained at 30 °C and pH 4.5 for the L-21G414 and L-21ScaI ribozymes, respectively. These comparisons suggest that the results obtained from the L-21G414 ribozyme reaction with −1d,rS can be related to its reaction with rS by analogy to the L-21ScaI ribozyme reaction. Further, the observation of the same rate constants for reaction of exogenous G and the intramolecular G414 suggests that the same G-binding site is used in the first and second steps of self-splicing (see Discussion).

Determination of the Rate Constant for Substrate Dissociation (k_{off}^{S})

The rate constant of S dissociation (k_{off}^{S}) from the binary complex E^{G414}·S* was measured by a three-part pH-jump pulse−chase experiment (Figure 6A). Excess E^{G414} was incubated with −1d,rS* at pH 5.3 for t_1 = 1 min to allow the formation of the E^{G414}·S* complex (eq 7), followed by

$$\text{during } t_1\text{: } E^{G414} + S^* \overset{\text{fast}}{\rightleftharpoons} E^{G414}\cdot S^* \xrightarrow{\text{slow}} E^{G414A_5}\cdot P^* \quad (7)$$

addition of a chase solution containing a large excess of unlabeled P for various time t_2.

The low pH during the first two steps was designed to prevent conversion of E^{G414}·S* to E^{G414A_5}·P* and to allow the dissociation of S* to be followed: during t_2 when S* dissociates from E^{G414}, it cannot rebind because the free E^{G414} is trapped by unlabeled P (eq 8).

$$\begin{array}{l} \text{during } t_2\text{: } E^{G414}\cdot S^* \xrightarrow{\text{slow}} E^{G414A_5}\cdot P^* \\ \quad\quad\quad\quad \downarrow \text{fast} \\ \quad\quad\quad\quad E^{G414} + S^* \\ \quad\quad\quad\quad \overset{P}{\downarrow} \\ \quad\quad\quad\quad E^{G414}\cdot P^* \end{array} \quad (8)$$

At the end of each t_2, a high pH (8.2) chase solution allowed a constant fraction of the S* remaining bound to be rapidly converted to P* ($k_f \gg k_{off}^{S}$) (eq 9). As shown in

$$\text{during } t_3\text{: } E^{G414}\cdot S^* \overset{\text{very fast}}{\rightleftharpoons} E^{G414A_5}\cdot P^* \quad (9)$$

Figure 6B, the amount of P* formed decreased with increasing t_2, and a value of k_{off}^{S} = 1.4 min^{-1} was obtained. This value is in good agreement with the value of 1.2 min^{-1} calculated above.

Determination of Substrate and Product Association Rate Constants (k_{on}^{S} and k_{on}^{P})

k_{on}^{S}. Under subsaturating conditions, the binding of substrate (k_{on}^{S}) is rate-limiting if the rate of the chemical conversion is faster than the dissociation of substrate ($k_{off}^{S} \ll k_c$). This holds for reaction of rS with E^{ScaI} (Herschlag & Cech, 1990a; Herschlag et al., 1991a). However, there are difficulties in using −1d,rS to measure this rate constant. (1) As shown above, k_{off}^{S} and k_f of −1d,rS are similar so that E^{G414}·S* partitions between dissociation and formation of product. (2) At the low E^{G414} concentration required to establish subsaturating conditions for −1d,rS, the reaction is so slow that the subsequent dissociation of P also contributes to the reaction, rendering the reaction non-first-order.

The all-ribose substrate (rS) was therefore used to measure k_{on}^{S}; for rS, the chemical step is very fast compared to substrate dissociation ($k_f \gg k_{off}^{S}$).[3] The observed rate constant was measured with subsaturating concentrations of E^{G414} (5−30 nM), and the second-order rate constant k_{on}^{S} = 0.5 × 10^8 M^{-1} min^{-1} was obtained from the slope of the plot of the observed rate constant vs E^{G414} concentration (data not shown; the concentrations of E^{G414} used that exceed K_d^S are not saturating because of the rapid conversion of bound S to P, analogous to the steady-state situation in which $K_m > K_d$). Previous studies with E^{ScaI} have demonstrated that a deoxyribose substitution at the −1 or other positions does not significantly affect the rate of substrate binding (Herschlag et al., 1993a,b). Qualitative results for k_{on}^{S}

[3] $k_f \approx 200$ $min^{-1} \gg k_{off}^{S} \approx 1$ min^{-1}. The value of k_f was obtained from rS reacting with E^{ScaI} and the value of k_{off}^{S} was obtained from −1d,rS dissociating from E^{G414} or E^{ScaI}; rS dissociates even more slowly (~2.5-fold) than −1d,rS from E^{ScaI} (Herschlag & Cech, 1990; Herschlag et al., 1993b).

obtained with E^{G414} and −1d,rS (not shown) suggest that this also holds for E^{G414}.

$$E^{G414} + S^* \overset{k_{on}^S}{\rightleftharpoons} E^{G414}\cdot S^* \overset{\text{fast}}{\rightleftharpoons} E^{G414A_5}\cdot P^* \quad (10)$$

k_{on}^P. To obtain the rate constant for P binding, the E^{G414A_5} form of the ribozyme is required. Labeled $E^{G414A_5p^*Ap}$ was generated by using 3′-labeled S and purified by denaturing PAGE (see Materials and Methods). The all-ribose oligonucleotide version of P was used for the reasons described above for S. The observed rate constant for formation of $E^{G414A_5p^*Ap}\cdot P$ was measured with a set of subsaturating concentrations of unlabeled rP (2−10 nM) which was added to ~0.1 nM $E^{G414A_5p^*Ap}$. A second-order rate constant of $k_{on}^P = 0.2 \times 10^8$ M^{-1} min^{-1} was obtained from the slope of the plot of observed rate constant vs P concentration (not shown).

$$E^{G414A_5p^*Ap} + P \overset{k_{on}^P}{\rightleftharpoons} E^{G414A_5p^*Ap}\cdot P \rightleftharpoons E^{G414}\cdot S^* \rightharpoonup E^{G414} + S^* \quad (11)$$

Determination of the Rate Constant for Dissociation of Product (k_{off}^P)

A pulse−chase experiment, essentially as described above in Figure 4A, was used to determine the rate constant for dissociation of P. The central feature of this experiment is that P* that dissociates is trapped by E^{G414} (eq 3 and above). In contrast, S* that dissociates rebinds the large excess of E^{G414} and is converted to P* that can subsequently be trapped by E^{G414} (eq 3; see above). Thus, P* slowly accumulates during t_1, gradually perturbing the plateau in Figure 7A (closed symbols). At various t_1, a high pH (8.2) chase solution with a large excess of unlabeled P was added. During t_2, the high pH ensured that bound P* was rapidly converted to S*, and the dissociation of S*, which is faster than that of P*, allowed essentially all bound P* to accumulate as free S* (eq 2). This is confirmed by the nearly complete regeneration of S* at the shorter t_1's (Figure 7A, open circles). Thus, the amount of bound P* remaining at the end of t_2 decreased with increasing t_1, and this difference represents the amount of P* that had dissociated during t_1. This is plotted in Figure 7B and gives $k_{obs} = 0.003$ min^{-1}, from which $k_{off}^P = 0.007$ min^{-1} is obtained [$k_{off}^P = [(1 + K_{int})/K_{int}]k_{obs}$]. The slow phase of bound S* decrease (Figures 4B and 7A, closed circles) can also be used as a measure of the rate constant of P* dissociation. It gives an identical rate constant.

Visualization of the Dissociation of P and S. A gel mobility shift method was employed to visualize the dissociation of P and S and to test predictions from the overall kinetic and thermodynamic framework for the E^{G414} ribozyme reaction. Pulse−chase experiments were performed analogously to those described above (Figure 4A), except that the samples were directly loaded onto a native gel at various time t_2. In the previous experiments, samples were analyzed by denaturing gel electrophoresis to assay the total amount of S* and P* present. In this experiment, a native gel was employed to separate bound S* and P* from free S* and free P*.

The denaturing assays described above suggested that the internal equilibrium between bound S* and bound P* is rapidly established. Native gel analysis confirmed this conclusion, showing that >90% of the labeled S and P migrated with the ribozyme as a single slowly migrating band (Figure 8A, $t_2 = 0$). Following a chase with an excess of unlabeled P, there is an initial fast phase of S* dissociation followed by a slower release of more S*, with no significant formation of free P* (Figure 8A). These results are predicted from the reaction framework of Scheme 1 as follows. The fast phase is consistent with dissociation of the 0.6 of the label present as $E^{G414}\cdot S^*$, and the slow phase is consistent with conversion of the 0.4 of the label present as $E^{G414A_5}\cdot P^*$ to $E^{G414}\cdot S^*$ followed by dissociation of S*; S* dissociates instead of P* because $k_{off}^S \gg k_{off}^P$ (eq 2).

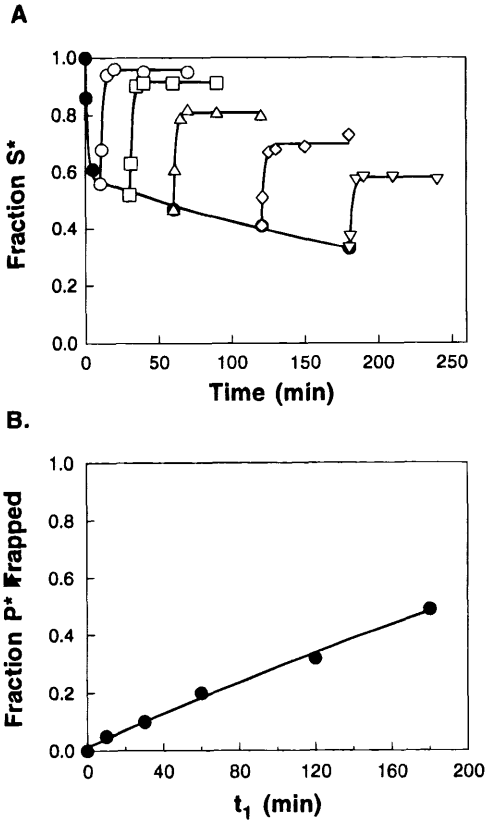

FIGURE 7: Determination of the rate constant for dissociation of product from E^{G414A_5} (k_{off}^P). (A) The pulse−chase protocol followed that outlined in Figure 4A, except that a higher pH chase (8.2) was used to ensure rapid and quantitative conversion of the P* remaining bound to S*. E^{G414} (100 nM) was incubated with ~0.1 nM −1d,S* (10 mM $MgCl_2$ and 50 mM sodium MES, pH 6.8) for various times t_1 to establish the internal equilibrium and to allow subsequent dissociation of P* (see text) and was then diluted 10-fold with a chase solution containing 5 μM unlabeled P, 10 mM $MgCl_2$, and 50 mM EPPS, pH 8.2, for t_2. The closed symbol (●) represents the fraction of S* as a function of t_1 (i.e., $t_2 = 0$), and the open symbols represent the fraction of S* at times t_2 after chases initiated at the indicated t_1 times: $t_1 = 10$ min (○), 30 min (□), 60 min (△), 120 min (◇), and 180 min (▽). (B) Fraction of P* that is not converted to S* during t_2. This corresponds to the fraction of P* trapped by E^{G414} during t_1. The curve in B represents a nonlinear least-squares fit to the data. The curves in part A were obtained as described in the legend to Figure 4. The curve in B and the second phase of the curve through the closed symbol in A give $k_{obs} = 0.003$ min^{-1}, from which $k_{off}^P = 0.007$ min^{-1} is derived [$k_{off}^P = k_{obs}/(1 + K_{int})/K_{int}$]. The curves through the open symbols give values of $k_{obs} = 0.45-0.69$ min^{-1} for regeneration of S*. These rate constants are faster than the corresponding rate constant in Figure 4B because the higher pH used in Figure 7 speeds the conversion of bound P* to S*.

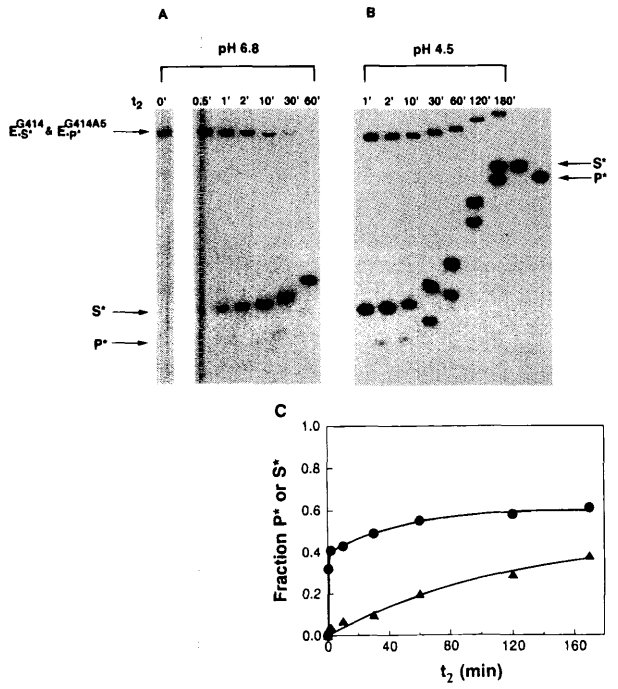

FIGURE 8: Visualization of substrate and product dissociation by gel mobility shift. A pulse–chase protocol was followed, in which the internal equilibrium was first established at pH 6.8 (100 nM E^{G414}, ~0.1 nM 5′-labeled −1d,rS, 10 mM $MgCl_2$, 50 mM sodium MES; t_1 = 10 min), followed by addition of a chase solution containing excess unlabeled P at pH 6.8 (A) or pH 4.5 (B). Aliquots taken at various times t_2 were mixed with loading solution and immediately loaded onto a running native gel (see Materials and Methods). S* and P* correspond to standards, −1d,rS* and −1d,rP*, respectively, loaded at the end of the experiment. The apparent differences in migration are due to different loading times. The fraction of free −1d,rS* (●) and −1d,rP* (▲) formed after addition of chase in part B is plotted as a function of t_2, with the latter giving a rate constant of k_{obs} = 0.005 min^{-1} (C) and k_{off}^{P} = 0.01 min^{-1}, as described in the legend to Figure 7. The −1d,rP* curve is a nonlinear least-squares fit to the data.

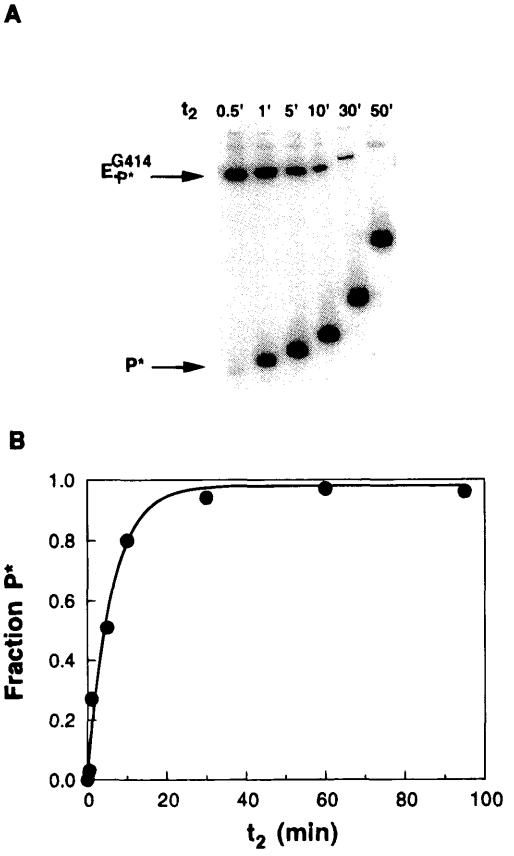

FIGURE 9: Determination of rate constant for P dissociation from E^{G414}. (A) A gel mobility shift experiment, as described in the legend to Figure 8A, except that E^{G414} was mixed with −1d,rP* instead of with −1d,rS* so that dissociation of the E^{G414}·P* complex was followed. (B) The fraction of free −1d,rP* formed as a function of time t_2 following the chase with an excess of unlabeled P. The curve represents a nonlinear least squares fit to the data and gives a rate constant of k_{off}^{P} = 0.1 min^{-1}.

In a second related experiment, a low-pH chase (4.5) was used to inhibit re-formation of E^{G414}·S* from E^{G414A_5}·P* (eq 12; Figure 8B). In this case, a slow accumulation of P* was observed subsequent to the rapid release of S*, consistent with the conclusion that k_{off}^{P} is much less than k_{off}^{S}. The rate constant for dissociation of P of ~0.01 min^{-1} obtained from Figure 8C is similar to the value of k_{off}^{P} = 0.007 min^{-1} obtained above at pH 6.8. This experiment confirms the very slow dissociation of P and suggests that the dissociation is largely insensitive to pH.

Interactions Responsible for the Strong Binding of P

Product dissociates from E^{G414A_5} about 40-fold more slowly than from the L-21ScaI ribozyme (Table 1). The differences between these two ribozyme forms are the 3′-pA_5 tail that was transferred from S to the G414-containing ribozyme and the five 3′-terminal residues present in the L-21G414 ribozyme but not the L-21ScaI ribozyme (Figure 2B,C). To identify which of these components contributes to the additional stabilization of bound P, the rate of dissociation of P* from E^{G414A_5} and E^{G414} was compared. The pulse–chase gel mobility shift experiment described in Figure 8 was repeated, except that E^{G414} was mixed with P* instead of S*. This allowed dissociation of P* from the E^{G414}·P* complex to be monitored (Figure 9A). The dissociation of P* from E^{G414} is much faster than from E^{G414A_5} (Figure 9A vs Figure 8A) and gives a dissociation rate constant of $k_{off}^{P}{}'$ = 0.1 min^{-1} (Figure 9B). This is about 15-fold greater than that of the E^{G414A_5}·P* complex (Table 1), suggesting that the ribozyme's pA_5 tail is largely responsible for the slow dissociation. In contrast, the values of $k_{off}^{P}{}'$ for dissociation of P from E^{G414} and E^{ScaI} are similar (Table 1),[4] suggesting that the terminal five residues of the intron, including the 3′ portion of P9.0 and the 3′-terminal G414, do not have a large effect on binding of P.

Competition between Exogenous G and the 3′-Terminal G414 for the G-Site

The same value of k_f for the L-21ScaI and the L-21G414 ribozyme reactions suggests that the 3′-terminal residue G414 is predominantly docked into the G-binding site. The

[4] Though E^{G414} contains G in the G-binding site whereas E^{ScaI} does not, the presence of bound G was previously shown to have only a small effect of ~2-fold on binding of P to E^{ScaI} (McConnell et al., 1993; Bevilacqua et al., 1993).

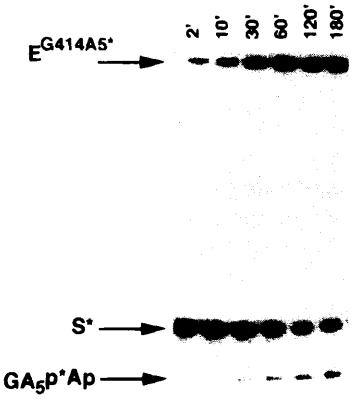

FIGURE 10: Exogenous G does not compete effectively with the 3′-terminal G414. Reaction of 100 nM E^{G414} with 0.1 nM 3′-labeled −1d,rS (CCCUCdUA$_5$p*Ap) was carried out in the presence of 2.5 mM G, 10 mM $MgCl_2$, and 50 mM sodium MES, pH 5.3, at 50 °C for the indicated times. The product of 3′-terminal G414 as nucleophile is 3′-labeled ribozyme $E^{G414A_5p^*Ap}$ and the product of the exogenous G is GA$_5$p*Ap.

occupancy of G414 in the G-binding site was further tested by a competition experiment in which intermolecular G was added to compete with the intramolecular G414. 3′-End-labeled oligonucleotide substrate was used in this experiment. If the ribozyme used the 3′-terminal G414 as the nucleophile, a 3′-labeled ribozyme, $E^{G414A_5p^*Ap}$, would be formed; if it used the exogenous G, GA$_5$p*Ap would be formed (eq 13).

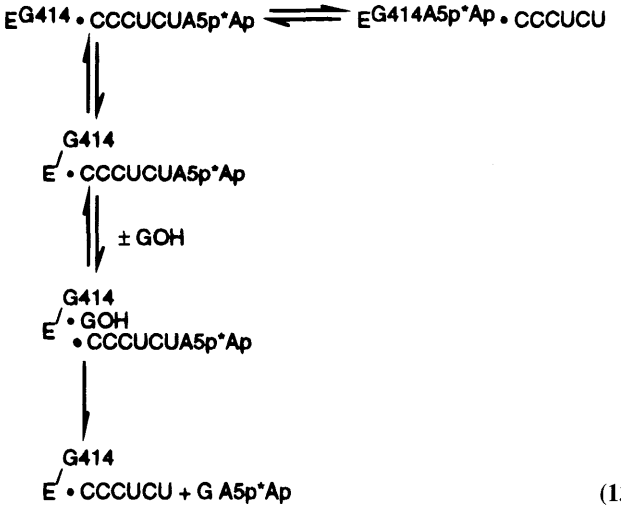

(13)

Reactions were carried out in the presence of 2.5 mM exogenous G, a concentration well above its dissociation constant with the L-21ScaI ribozyme ($K_d^G \approx 0.1$ mM; McConnell et al., 1993). As shown in Figure 10, the only product observed at early times is $E^{G414A_5p^*Ap}$, the product from reaction with G414. As bound oligonucleotide substrate and product are in equilibrium and interconverting (eq 13), exogenous G has multiple opportunities to react with the labeled oligonucleotide substrate. The product from the exogenous G reaction, GA$_5$p*Ap, was observed after long incubation times (Figure 10). Analogous results were obtained at different pHs and in the presence of 20 mM GMP (not shown). The ~100-fold slower formation of the exogenous G product (not shown) sets an upper limit on the fraction of time that G414 spends out of the G binding site. This value is an upper limit because the slow reaction with exogenous G could be catalyzed by a small fraction of damaged ribozyme that lacks the 3′-terminal G414 residue. In summary, exogenous G cannot compete effectively with the intramolecular G414 residue, suggesting that the E^{G414} ribozyme exists predominantly with G414 docked in the G binding site.

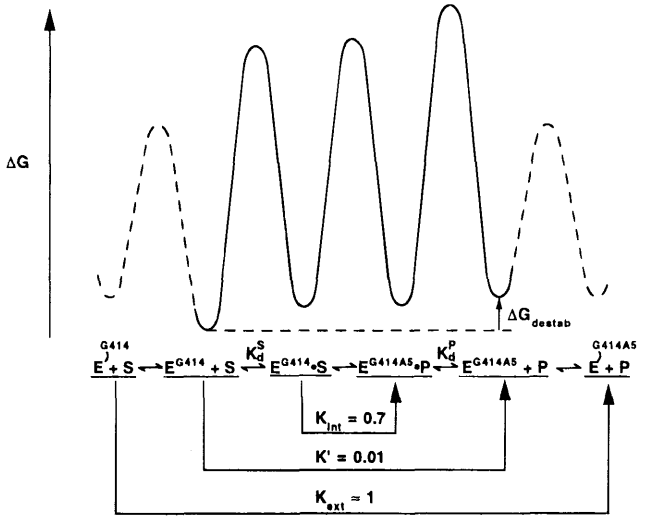

FIGURE 11: Free energy-reaction profile for the L-21G414 ribozyme and −1d,rS (10 mM $MgCl_2$, pH 6.8, 50 °C). A standard state of 1 nM reactants and products was chosen; the relative free energies were obtained from the rate and equilibrium constants in Scheme 1 and an assumed value of $K_{ext} = 1$ for the overall phosphoryl transesterification reaction (see Results). The absolute values of equilibrium constants for docking of the intramolecular G414 or G414A$_5$ into the ribozyme's active site are not known and are therefore depicted with dashed lines. However, the relative free energy for docking of G414 vs G414A$_5$ is obtained from this free energy-reaction profile. Docking of G414A$_5$ is more difficult than that of G414. A model for the origin of this destabilization is described in the Discussion.

Free Energy-Reaction Profile

A free energy profile for the L21-G414 ribozyme reaction with −1d,rS was obtained from the rate and equilibrium constants of Scheme 1 (Figure 11). The conversion to free energy was obtained according to the equations $\Delta G = -RT \ln K$ and $\Delta G^{\ddagger} = -RT \ln (hk/k_BT)$, where R is the gas constant, T is temperature in K, h is Planck's constant, and k_B is the Boltzmann constant. The profile was formulated as follows. First, relative energies for E^{G414}•S and E^{G414A_5}•P and the barrier for their interconversion was obtained from K_{int}, k_f, and k_r. Second, the height of activation energy barriers for S and P dissociation were determined from k_{off}^S and k_{off}^P, respectively. Next, the free energies of S + E^{G414} and P + E^{G414A_5} relative to the level of the activation barriers for S and P dissociation were determined from the association rate constants, k_{on}^S and k_{on}^P; a standard state of 1 nM reactants and products was used.

Finally, the free energy values were related to the overall reaction equilibrium. To do this, two hypothetical species were defined, $E^{/G414}$ and $E^{/G414A5}$. These species represent the E^{G414} and E^{G414A_5} forms of the ribozyme with the 3′ terminus flipped out of the active site. Thus, the energies of G414 (+S) and G414A$_5$ (+P) follow the energetics of a simple phosphoryl transesterification in solution. A value of $K_{ext} = 1$ is assumed for the transesterification in the free energy profile.[5] Thus, the free energy levels of {$E^{/G414}$ + S} and {$E^{/G414A5}$ + P} are the same. However, the energy

of these species relative to those in the central portion of Figure 11 is not known. The "docking" of G414 into the active site is depicted as energetically downhill, because the 3′-terminal G of E^{G414} appears to exist predominantly occupying the guanosine binding site (see Discussion).

Relating the external equilibrium to the energies of the docked and bound states indicates that docking of $G414A_5$ is ~100-fold harder than docking of G414. This is seen in the relative docking equilibria: $K_{dock}^{G414}/K_{dock}^{G414A5}$ {$= ([E^{G414}]/[E'^{G414}])/([E^{G414A_5}]/[E'^{G414A5}]) = K_{ext}/K'$}. Similarly, the species {$E^{G414} + S$} is favored over {$E^{G414A_5} + P$} by 100-fold (Figure 11, $K' = 0.01 = ([E^{G414A_5}][P])/([E^{G414}][S]) = (k_{on}^{S}k_{f}k_{off}^{P})/(k_{off}^{S}k_{r}k_{on}^{P}) = 0.01$. This latter comparison is independent of the assumption of $K_{ext} \approx 1$. A model for the origin of the destabilization of E^{G414A_5} relative to E^{G414} is described in the Discussion.

DISCUSSION

The L-21G414 ribozyme contains the 3′-terminal G and P9.0 duplex, features involved in the second step of group I self-splicing (Figure 2C). As these components are absent in the previously characterized L-21ScaI ribozyme (Figure 2B), comparison of the kinetic and thermodynamic framework for these ribozymes allows a stepwise approach toward understanding the second step of self-splicing (Scheme 1, Figure 11, and Table 1). This comparison has elucidated the behavior of the intramolecular G nucleophile, which is used in the second step of self-splicing, relative to the behavior of exogenous G, which is used in the first step of self-splicing (Figure 1). The framework and the ability to study the reaction in both directions have led to mechanistic insights. Finally, the results provide new information, as well as raise new questions about how the group I intron ensures efficient ligation of exons.

Kinetic Evidence for a Single G Binding Site. Self-splicing of group I pre-rRNA occurs through two sequential steps (Figure 1A). Exogenous G is used as the nucleophile in the first step and a universally conserved 3′ terminus G residue of the intron is used in the second step (Cech, 1990). These steps are chemically the reverse of each other, with the bound exogenous G nucleophile in the first step equivalent to the 3′-terminal G leaving group in the second step. This led to the proposal that a single G binding site was used in both steps (Inoue et al., 1986), though a model with two distinct sites was also proposed (Kay et al., 1988). More recent results have provided strong support for the single site model. Whereas the wild-type intron has a preference for exogenous G over A in the first step of self-splicing and for a 3′-terminal G over A residue in the second step, mutation of a single base pair in the ribozyme's core switches this preference to A over G in both steps (Michel et al., 1989; Been & Perrotta, 1991).

Comparison of the reactivity of exogenous G with that of the intramolecular 3′-terminal G provides a further test of this model. The rate of the chemical step for reactions of the L-21 ScaI ribozyme with bound exogenous G and the L-21G414 ribozyme with its 3′-terminal G were the same, within experimental uncertainty, under various conditions of changing pH, temperature, and oligonucleotide substrate identity (Table 3 and Results). These data strongly support the single site model and further suggest that the overall active site architecture and orientation remain the same in both steps. An unlikely coincidence would be required to allow the same rate of reaction from different or overlapping binding sites.

Evolution of a single binding site is expected to be more probable than evolution of two distinct or partially distinct sites. The intron has apparently taken advantage of the same G binding site in both self-splicing steps. This evolutionary perspective also answers a related question: Why did the intron "choose" exogenous G as a cofactor in the first step? Chemically, the nucleophilicity of the 3′-OH of G is essentially the same as the hydroxyl groups of of other nucleosides, sugars, and water, and water is present at much higher concentrations. Indeed, group I introns can self-splice *in vitro* in the absence of G by using water in the first reaction step [e.g., Inoue et al. (1986)]. However, once G was chosen as the residue that defines the 3′ splice site, that same G binding site could be used to facilitate 5′ splice site cleavage in the first step. The first step of self-splicing is faster in the presence of G than in its absence, suggesting that the intron uses binding interactions with the G for positioning the 3′-OH and perhaps functional groups such as the 2′-OH to help activate the 3′-OH (Bass & Cech, 1986). The evolution of the single G binding site that is used in two successive steps is presumably analogous to the situation for the protein enzymes galactose-1-P uridylyltransferase and nucleoside diphosphate kinase. These enzymes use a single substrate binding site and covalent catalysis to transfer a uridyl phosphate or phosphate group between group acceptors that are sterically and electrostatically similar (Sheu et al., 1979). In contrast, the use of a 2′-OH nucleophile in the first reaction step and a 3′-OH leaving group in the second step of the group II self-splicing reaction and comparison of the thiophosphate discrimination in the first and second steps suggest differences in the binding modes or active sites between the two steps [Padgett et al., 1994; Podar et al., 1995; see also Moore and Sharp (1993)].

The 3′-Terminal G Is Predominantly Docked in the G Binding Site. The similar rate constants for reaction of the 3′-terminal G414 of the L-21G414 ribozyme and the exogenous G bound to the L-21 ScaI ribozyme also suggest that the 3′-terminal G of the G414-containing ribozyme is in the G binding site (i.e., that the equilibrium for docking of the G414 favors the docked form). A slower rate for the L-21G414 reaction would be expected if G414 were undocked and out of the active site a significant fraction of the time. The inability of exogenous G to compete with G414 (Figure 10) further suggests that the intramolecular G is predominantly docked in the G binding site. This high occupancy may be important for ensuring accuracy in the choice of the 3′ splice site during self-splicing and in preventing spurious side reactions.

A Thermodynamic Barrier for $G414A_5$ Docking: A Model of Substrate Destabilization. The free energy-reaction profile

[5] A value of $K_{ext} = [P][GA]/[S][G] = 4$ has been observed for the analogous reaction with the all-ribose oligonucleotide substrate, CCCUCUA (T. S. McConnell, D. Herschlag, and T. R. Cech, unpublished results). Preliminary results suggest a value of $K_{ext} \approx 0.1$ for the reaction of CCCUCdUA [this value may differ from 1 because the transfer of a phosphoryl group from dU to rG is no longer fully symmetrical in the vicinity of the phosphoryl group (T. S. McConnell, D. Herschlag, and T. R. Cech, unpublished results)]. Thus, there is significant uncertainty in the value of K_{ext}. The extent of this uncertainty, however, is not expected to alter the qualitative conclusions in the text.

for the L-21G414 reaction reveals that it is ~100-fold harder to dock G414 into its binding site when a pA_5 tail is attached (Figure 11). Similarly, the E^{G414A_5}·P form of the ribozyme is ~100-fold destabilized relative to the E^{G414}·S form ($K' = 0.01$). The internal equilibrium is unaffected by shortening this tail to a single A residue (unpublished results), and GA_5 and GA have the same k_{cat}/K_m for reaction in *trans* with the L-21ScaI ribozyme, suggesting that the terminal four A's are not responsible for the destabilization (T. S. McConnell, D. Herschlag, and T. R. Cech, unpublished results). The binding of unreactive 2′-deoxyribose G analogs also show 50-fold destabilization upon addition of the pN tail to dG (Moran et al., 1993), and kinetic studies indicate that GA binds at least 20-fold weaker than G to the L-21ScaI ribozyme (T. S. McConnell, D. Herschlag, and T. R. Cech, unpublished results).

This destabilization is reminiscent of results obtained previously for binding of the oligonucleotide substrate and product to the L-21 ScaI ribozyme. Piccirilli et al. (1993) obtained evidence for an interaction of this 3′-oxygen of the U leaving group with Mg^{2+} in the transition state from an oxygen/sulfur metal ion specificity switch experiment. It was subsequently shown that the reactive phosphoryl of the substrate destabilizes tertiary binding interactions by 40-fold relative to binding of the oligonucleotide product, which contains a 3′-OH group (Narlikar et al., 1995). The destabilization was attributed to weakening of the interaction of the 3′-oxygen of the U leaving group with the active site Mg ion upon attachment of the electron-withdrawing phosphoryl group to the 3′-oxygen. This led to a model for catalysis in which electrostatic destabilization of the ground state and electrostatic stabilization of charge accumulation on the 3′-oxygen of U in the transition state both contribute to lowering the barrier for reaction.

A second active site metal ion has been the subject of much discussion (Steitz & Steitz, 1993; Herschlag et al., 1993b; Yarus, 1993). One model involving a second Mg ion that interacts with the 3′-oxygen of G could account for the weaker docking of G414 when a phosphoryl group is attached to its 3′-oxygen. Such an interaction would be expected to be catalytic because bound G414pA (or exogenous phosphorylated G) would be destabilized and the partial negative charge that accumulates on the 3′-oxygen of G414 in the transition state would be stabilized. The presence of a second active site Mg ion is also consistent with the thermodynamic symmetry between bound substrates and products, as discussed in the next section. It should be emphasized, however, that there are other possible origins of this destabilization, including destabilization of G414pA by catalytic hydrogen bond donors and stabilization of G414 by nonproductive donation of a hydrogen bond from its 3′-hydroxyl group; there is no direct evidence for the presence of this second metal ion.

A Thermodynamically Matched Active Site ($K_{int} \approx 1$). The chemical step of the L-21G414 ribozyme reaction reaches an internal equilibrium near 1 ($K_{int} = k_f/k_r = [E^{G414A_5}\cdot P]/[E^{G414}\cdot S] = 0.7$ for the −1d,rS substrate; Table 2). The value of K_{int} is rather insensitive to the nature of the substrate. For example, $K_{int} = 1.5$, 0.71, and 1.0 were obtained for reactions of the all-ribose substrate $CCCUCUA_5$, of $CCCUCdUA_5$, and of CCCUCdUU, respectively (Results and unpublished results; the 3′ U of CCCUCdUU mimics the ligated exons, as the first residue of the 3′ exon is a U). Balanced internal thermodynamics ($K_{int} \approx 1$) have been proposed to be characteristic of catalytically optimized enzymes (Albery & Knowles, 1976, 1977; Burbaum & Knowles, 1989; Burbaum et al., 1989), though there may be different constraints in self-splicing imposed by the single-turnover and two-step nature of this reaction. The matched energetics are consistent with structural symmetry in an active site designed to catalyze phosphoryl transfer between chemically identical 3′-oxygen atoms via a symmetrical trigonal bipyramidal transition state.[6]

Thermodynamic Coupling between G414A and 5′ Exon Analogs. The 5′ exon analog, P (CCCUCU), dissociates from E^{G414A_5} 200-fold more slowly than the ligated exon analog, S ($CCCUCUA_5$), from E^{G414}. However, P dissociates from E^{G414} ~15-fold faster than from E^{G414A_5} (Table 1), indicating that an interaction of the pA_5 tail contributes

A. Inefficient self-splicing

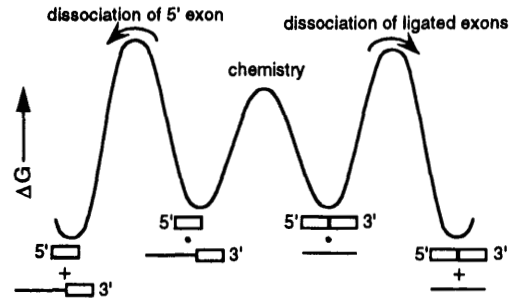

B. Thermodynamic model for efficient self-splicing

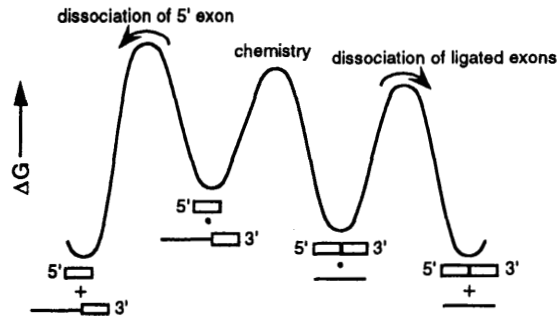

C. Kinetic model for efficient self-splicing

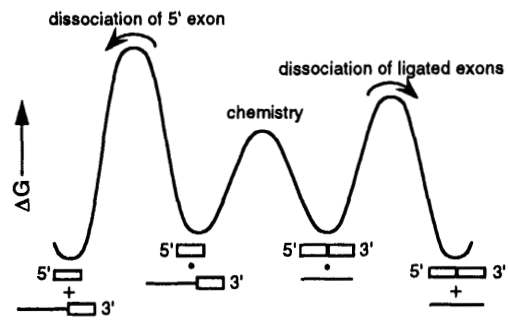

FIGURE 12: Models to ensure completion of the self-splicing reaction. Part A demonstrates that splicing would be inefficient with an internal equilibrium of 1 between bound ligated exons and bound 5′ exon and similar dissociation rates for the ligated exon species and the 5′ exon. Parts B and C show two solutions to this problem, changing the internal equilibrium to favor the ligated exon species (B, thermodynamic model) or slowing the release of the 5′ exon relative to the ligated exons (C, kinetic model). Exon sequences are depicted as open boxes and the intron as a line. The dot depicts bound species.

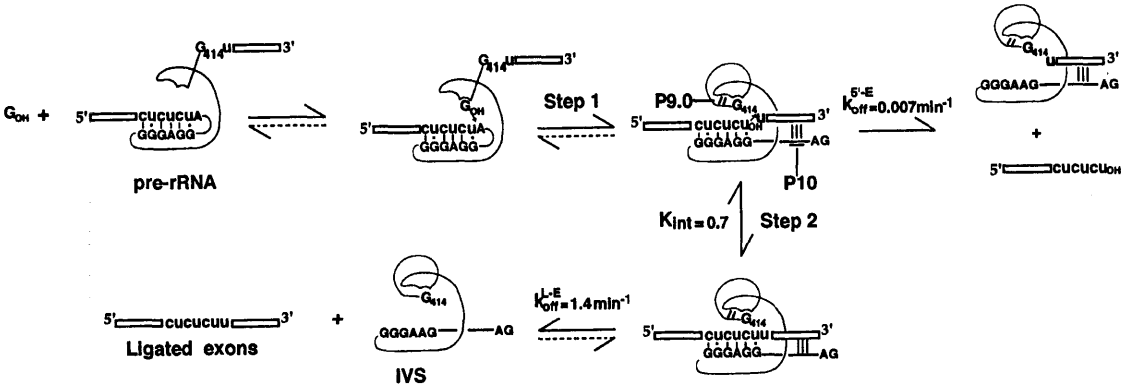

FIGURE 13: Kinetic control as a potential mechanism for completion of self-splicing. The rate and equilibrium constants listed were obtained in the L-21G414 reaction, which models the second step in self-splicing (Table 1). Note, however, that this ribozyme lacks the structural element P10 (Figure 2), which is expected to modulate the observed rates (see Discussion).

significantly to the slow dissociation. The observation of slow dissociation of P from E^{G414A} localizes the coupling to the 3′-pA (unpublished results). Thermodynamic coupling between binding of G and S was also localized to the 3′-pA, in this case to part of the oligonucleotide substrate S (McConnell et al., 1993). Preliminary experiments with substrates of varying sequence suggest that the A rather than the phosphate is responsible for the slow dissociation of P from E^{G414A} (unpublished results). In contrast, the similar rate of dissociation of P from E^{G414} and E^{ScaI} suggest that the 3′ residues of the intron, including residues required for P9.0 formation, do not contribute to the slow dissociation of 5′ exon analogs.

A Kinetic Mechanism To Ensure Completion of the Self-Splicing Reaction. The self-splicing reaction, as a simple phosphoryl transesterification reaction, might be expected to have an overall equilibrium near 1. This raises a question: what is the thermodynamic driving force that allows accumulation of ligated exons? The simplest answer is that the thermodynamic driving force is provided by the high concentration of G relative to the RNA *in vivo* (Cech, 1990). Structural changes over the course of self-splicing and subsequent reaction of the free intron may also help drive the reaction thermodynamically.

Although there is a thermodynamic driving force for the overall reaction, a second question remains: how does the intron ensure that self-splicing is completed rather than aborted after the first step due to dissociation of the 5′ exon from the 5′ exon·intron−3′ exon intermediate? It was previously noted that the tertiary binding interactions with the 5′ exon may play the biological role of preventing its dissociation and allowing sufficient time for the exon to attack at the 3′ splice site in the second step of self-splicing (Herschlag & Cech, 1990b). However, the tertiary binding interactions that slow the release of the 5′ exon should also slow the release of the ligated exons, as the 5′ exon is a component of the ligated exons. Thus, strong binding of the 5′ exon is a necessary but not sufficient criterion for efficient exon ligation.

The problem is illustrated by the hypothetical free energy-reaction profile in Figure 12A. In this case, splicing is inefficient even though the 5′ exon is bound tightly. This is because the ligated exons are bound just as tightly as the 5′ exon and the equilibrium between bound 5′ exon and bound ligated exons is 1. Thus, there is an equal probability for dissociation of ligated exons and 5′ exon, and only half of the RNA precursors yields ligated exons.

Figure 12 panels B and C present two possible solutions to this problem. In the thermodynamic model in Figure 12B, the 5′ exon and ligated exons still dissociate with the same rate constant, but efficient ligation is ensured by perturbing the internal equilibrium to favor bound ligated exons. Little bound 5′ exon dissociates since it does not accumulate. In contrast, the kinetic model in Figure 12C allows an internal equilibrium of unity with loss of the 5′ exon prevented by a larger kinetic barrier for its release than for release of the ligated exons.

Figure 13 shows the self-splicing reaction with the pertinent rate constants obtained from this study of the L-21G414 ribozyme. The internal equilibrium near 1 and the 200-fold slower release of the 5′ exon analog, P (CCCUCU), than of the ligated exon analog, S (CCCU-CUA_5), are consistent with the kinetic model in Figure 12C. The slow release of the 5′ exon may be likened to the strong binding of reaction intermediates to protein enzymes, which is presumably involved in ensuring completion of these reactions and preventing the release of reactive intermediates [e.g., Pompliano et al. (1990) and Kato et al. (1994)].

The slower release of the 5′ exon analog than of the ligated exon analog is maintained when CCCUCUU is used as the ligated exon analog (unpublished results). U is the 5′ residue of the 3′ exon in *Tetrahymena thermophila* pre-rRNA. However, other differences remain between this initial ribozyme model for the second self-splicing step and the actual self-splicing system. The most profound difference is the absence of P10 in the L-21G414 ribozyme (Figure 2A,C). This helix formed between the intron's IGS and the 5′ end of 3′ exon provides additional base pairing interactions with the ligated exons but not with the 5′ exon. It is thus most simply expected to *slow* the dissociation of the ligated exons. Indeed, as there is potential to form six Watson−Crick base pairs in P10, the effect is expected to be large

[6] It is observed that different energetic contributions to catalysis from the 2′-OH groups of the G and U are directly involved in the phosphoryl transfer (Bass & Cech, 1986; Tanner & Cech, 1987; Herschlag et al., 1993b; G. J. Narlikar and D. Herschlag, unpublished results). This observation suggests that there is not complete structural symmetry in the active site. Farther from the reactive phosphoryl group, the base of U is positioned in a G·U wobble pair, whereas the base of the attacking G is positioned by an interaction with a G·C pair and other interactions in P7 of the ribozyme's core (Michel et al., 1989; Yarus et al., 1991a,b; Doudna et al., 1989; Knitt et al., 1994; Strobel & Cech, 1993, 1994).

(Figure 2A). The problem of how the intron ensures the release of the ligated exon species rather than the 5′ exon is thus reintroduced.

These additional interactions also present a second kinetic problem—the release of the ligated exons within a physiologically relevant time frame. The six P10 base pairs are predicted to slow ligated exon release by $\sim 10^4$-fold (Freier et al., 1986). The predicted half-life for dissociation is then on the order of days at 50 °C (our experimental conditions) and even slower at physiological temperatures. It remains to be determined whether features intrinsic to the intron are responsible for speeding this dissociation or whether the assistance of cellular components is required, such as proteins acting as RNA chaperones.

ACKNOWLEDGMENT

We thank Geeta Narlitear and Deborah Knitt for discussions and Tom Cech and members of the Herschlag lab for critical reading of the manuscript.

REFERENCES

Albery, W. J., & Knowles, J. R. (1976) *Biochemistry 15*, 5631−5640.
Albery, W. J., & Knowles, J. R. (1977) *Angew. Chem., Int. Ed. Engl. 16*, 285−293.
Bass, B. L., & Cech, T. R. (1986) *Biochemistry 25*, 4473−4477.
Been, M. D., & Perrotta, A. T. (1991) *Science 252*, 434−437.
Bevilacqua, P. C., & Turner, D. H. (1991) *Biochemistry 30*, 10632−10640.
Bevilacqua, P. C., Johnson, K. A., & Turner, D. H. (1993) *Proc. Natl. Acad. Sci. U.S.A. 90*, 8357−8361.
Bruce, A. G., & Uhlenbeck, O. C. (1978) *Nucleic Acids Res. 5*, 3665−3677.
Burbaum, J. J., & Knowles, J. F. (1989) *Biochemistry 28*, 9306−9313.
Burbaum, J. J., Raines, T., Albery, J. W., & Knowles, J. F. (1989) *Biochemistry 28*, 9293−9305.
Burke, J. M., Esherick, J. S., Burfeind, W. R., & King, J. L. (1990) *Nature 344*, 80−82.
Cech, T. R. (1990) *Annu. Rev. Biochem. 59*, 543−568.
Cech, T. R., Herschlag, D., Piccirilli, J. A., & Pyle, A. M. (1992) *J. Biol. Chem. 267*, 17479−17482.
Doudna, J. A., Cormack, B. P., & Szostak, J. W. (1989) *Proc. Natl. Acad. Sci. U.S.A. 86*, 7402−7406.
Freier, S. M., Kierzek, R., Jaeger, J. A., Sugimoto, N., Caruthers, M., Nielson, T., & Turner, D. H. (1986) *Proc. Natl. Acad. Sci. U.S.A. 83*, 9373−9377.
Herschlag, D., & Cech, T. R. (1990) *Biochemistry 29*, 10159−10171.
Herschlag, D., & Khosla, M. (1994) *Biochemistry 33*, 2591−2597.
Herschlag, D., Piccirilli, J. A., & Cech, T. R. (1991) *Biochemistry 30*, 4844−4854.
Herschlag, D., Eckstein, F., & Cech, T. R. (1993a) *Biochemistry 32*, 8299−8311.
Herschlag, D., Eckstein, F., & Cech, T. R. (1993b) *Biochemistry 32*, 8312−8321.
Inoue, T., Sullivan, F. X., & Cech, T. R. (1986) *J. Mol. Biol. 189*, 143−165.
Kato, H., Tanaka, T., Vamaguchi, H., Hara, T., Nishioka, T., Yukiteru K., & Oda, J. (1995) *Biochemistry 33*, 4995−4999.
Kay, P. S., Menzel, P., & Inoue, T. (1988) *EMBO J. 7*, 3531−3537.
Knitt, D. S., & Herschlag, D. (1996) *Biochemistry 35*, 1560−1570.
Knitt, D. S., Narlikar, G. J., & Herschlag, D. (1994) *Biochemistry 33*, 13864−13879.
Lambowitz, A. M. (1993) *Annu. Rev. Biochem. 62*, 587−622.
Lehman, N., & Joyce, G. F. (1993) *Nature 361*, 182−185.
McConnell, T. S., Cech, T. R., & Herschlag, D. (1993) *Proc. Natl. Acad. Sci. U.S.A. 90*, 8362−8366.
Michel, F., & Westhof, E. (1990) *J. Mol. Biol. 216*, 585−610.
Michel, F., Jacquier, A., & Dujon, B. (1982) *Biochimie 64*, 867−881.
Michel, F., Hanna, M., Green, R., Bartel, D. P., & Szostak, J. W. (1989) *Nature 342*, 391−395.
Moore, M. J., Sharp, P. A. (1993) *Nature 365*, 364−368.
Moran, S., Kierzek, R., & Turner, D. H. (1993) *Biochemistry 32*, 5247−5256.
Narlikar, G. J., Gopalakrishnan, V., McConnell, T. S., Usman, N., & Herschlag, D. (1995) *Proc. Natl. Acad. Sci. U.S.A. 92*, 3668−3672.
Padgett, R. A., Podar, M., Boulanger, S. C., & Perlman, P. S. (1994) *Science 266*, 1685−1688.
Podar, M., Perlman, P. S., & Padgett, R. A. (1995) *Mol. Cell. Biol. 15*, 4466−4478.
Pompliano, D. L., Peyman, A., & Knowles, J. R. (1990) *Biochemistry 29*, 3186−3194.
Pyle, A. M., McSwiggen, J. A., & Cech, T. R. (1990) *Proc. Natl. Acad. Sci. U.S.A. 87*, 8187−8191.
Rajagopal, J., Doudna, J. A., & Szostak, J. (1989) *Science 244*, 692−694.
Robertson, D. L., & Joyce, G. F. (1990) *Nature 344*, 467−468.
Rose, I. A., O'Connell, E. L., Litwin, S., & BarTana, J. (1974) *J. Biol. Chem. 249*, 5163−5168.
Sheu, H. F. R., Richard, J. P., & Frey, P. A. (1979) *Biochemistry 18*, 5548−5556.
Steitz, T. A., & Steitz, J. A. (1993) *Proc. Natl. Acad. Sci. U.S.A. 90*, 6498−6502.
Strobel, S. A., & Cech, T. R. (1993) *Biochemistry 32*, 13593−13604.
Strobel, S. A., & Cech, T. R. (1994) *Nature Struct. Biol. 1*, 13−17.
Tanner, N. K., & Cech, T. R. (1987) *Biochemistry 26*, 3330−3340.
Tsang, J., & Joyce, G. F. (1994) *Biochemistry 33*, 5966−5973
Waring, R. B., & Davies, R. W. (1984) *Gene 28*, 277−291.
Woodson, S. A., & Cech, T. R. (1989) *Cell 57*, 335−345.
Yarus, M. (1993) *FASEB 7*, 31−39.
Yarus, M., Illangesekare, M., & Christian, E. (1991a) *Nucleic Acids Res. 19*, 1297−1304.
Yarus, M., Illangesekare, M., & Christian, E. (1991b) *J. Mol. Biol. 222*, 995−1012.
Zaug, A. J., & Cech, T. R. (1986a) *Science 231*, 470−475.
Zaug, A. J., & Cech, T. R. (1986b) *Biochemistry 25*, 4478−4482.
Zaug, A. J., Grosshans, C. A., & Cech, T. R. (1988) *Biochemistry 27*, 8924−8931.

BI9527653